International Journal of Thermophysics, Vol. 27, No. 4, July 2006 (© 2006)
DOI: 10.1007/s10765-006-0093-7

A New Instrument for the Measurement of the Thermal Conductivity of Fluids[1]

S. G. S. Beirão,[2] M. L. V. Ramires,[†,2] M. Dix,[3] and C. A. Nieto de Castro[2,4]

The transient hot-wire technique is at present the best technique for obtaining standard reference data for the thermal conductivity of fluids. It is an absolute technique, with a working equation and a complete set of corrections reflecting departures from the ideal model, where the principal variables are measured with a high degree of accuracy. It is possible to evaluate the uncertainty of the experimental thermal conductivity data obtained using the best metrological recommendations. The liquids proposed by IUPAC (toluene, benzene, and water) as primary standards were measured with this technique with an uncertainty of 1% or better (95% confidence level). Pure gases and gaseous mixtures were also extensively studied. It is the purpose of this paper to report on a new instrument, developed in Lisbon, for the measurement of the thermal conductivity of gases and liquids, covering temperature and pressure ranges that contain the near-critical region. The performance of the instrument for pressures up to 15 MPa was tested with gaseous argon, and measurements on dry air (Synthetic gas mixture, with molar composition certified by Linde AG, Wiesbaden, Germany, Ar – 0.00920; O_2 – 0.20966; N_2 – 0.78114), from room temperature to 473 K and pressures up to 10 MPa are also reported. The estimated uncertainty is 1%.

KEY WORDS: air; argon; fluids; thermal conductivity; transient hot-wire.

[†] Deceased

[1] Paper presented at the Seventeenth European Conference on Thermophysical Properties, September 5–8, 2005, Bratislava, Slovak Republic.

[2] Departamento de Química e Bioquímica and Centro de Ciências Moleculares e Materiais, Faculdade de Ciências da Universidade de Lisboa, Campo Grande, 1749-016 Lisboa, Portugal.

[3] Imperial College of Science and Technology, London, United Kingdom.

[4] To whom correspondence should be addressed. E-mail: cacastro@fc.ul.pt

1. INTRODUCTION

The measurement of the thermal conductivity of gases and liquids at low and moderate temperatures can now be undertaken with very good accuracy with the transient hot-wire technique, except near the critical point, where thermal gradients imposed by the method completely disturb the equilibrium state in a non-linear way, and at very low densities in the gaseous phase, where the number density of the gas is very small and the principles of the kinetic theory of gases are not obeyed.

Several instruments were developed in Lisbon, since the first apparatus for the measurement of the thermal conductivity of liquids using this technique [1–5] that was applied to liquid hydrocarbons. The second apparatus allowed studies at cryogenic temperatures, to measure liquefied gases, like argon and methane [6–9], and permitted measurements of a wide range of refrigerant liquids [10–13] that were environmentally acceptable. The need for accurate data on electrically conducting liquids justified the construction of the third apparatus, applied to the measurement of the thermal conductivity of water, and aqueous solutions of inorganic salts [14–16]. The quality of the data obtained, with uncertainties less than 0.5%,[1] permitted an international effort for the establishment of standard reference data for the thermal conductivity of toluene, *n*-heptane [17, 18], benzene [19], and water [20].

All these instruments did not have a wide pressure range. Taking advantage of the expertise developed with other authors, it was decided to develop a new thermal conductivity instrument, for measurements between room temperature and 300°C, and at pressures up to 70 MPa. It is the purpose of this paper to report on these developments.

2. THEORY OF THE METHOD

The theory of the transient hot wire is well known [21], and a complete uncertainty analysis has been presented previously [22]. The transient hot-wire method is an absolute method where the thermal conductivity of a fluid is evaluated by monitoring the rate at which the temperature of a thin wire increases with time after a step change of voltage has been applied to it. The constant heat flux per unit length thus generated by a linear source has the effect of producing throughout the fluid a temperature field that increases with time. According to the ideal mathematical model of an infinite line heat source, the thermal conductivity can be

[1] In the new formulation from ISO, the corresponding uncertainty with a coverage factor $k = 2$ would be approximately 1%.

obtained from the slope of the line ΔT_{id} vs. logarithm of time according to the following equation:

$$\Delta T_{id} = \frac{q}{4\pi\lambda} \ln \frac{4kt}{r_i^2 C}, \tag{1}$$

where q is the heat dissipation per unit length, λ is the thermal conductivity, t is the time, r_i is the radius of the wire, k is the thermal diffusivity, and C is equal to $\exp(\gamma)$ where γ is Euler's constant.

The global uncertainty of the experimental thermal conductivity obtained with the transient hot-wire method is a sum of a set of uncertainties related to three major contributions: deviations from the mathematical ideal model, presence of other modes of heat transfer like convection and radiation, and other random and systematic errors related with uncertainties of the measurement of some input quantities.

The first aspect mentioned above that contributes to the final uncertainty of the thermal conductivity experimental values is due to the deviations of the real model of the transient hot wire from the mathematical ideal model that refers to a infinite line source immersed in an infinite medium with properties independent of the temperature. Indeed, the finite diameter of the wire, its finite physical properties like the thermal conductivity or heat capacity, the fact that the wire has a finite length and must be suspended in some way and the finite boundaries of the fluid are some features that specify the real situation. Consequently, the experimental measurements of the temperature of the wire, ΔT_w, depart from the ideal temperature rise ΔT_{id}, predicted by Eq. (1) and a set of corrections must be added to the actual temperature rise;

$$\Delta T_{id} = \Delta T_w + \sum_i \delta T_i. \tag{2}$$

Two distinct situations can be considered: the effects can be minimized by a proper design of the instrument so the real behavior comes close to the ideal one – corrections smaller than 0.01% of ΔT_{id} – or, a number of small corrections have to be applied to the observed temperature rise of the wire to yield the linear dependence between the temperature increase of the wire and the logarithm of time. The various corrections δT_i have been studied exhaustively by various authors and are summarized elsewhere [21, 23]. Nevertheless, the contribution to the global uncertainty of the thermal conductivity by the uncertainties in these corrections never amount to more than 0.1% of the thermal conductivity.

The presence of other modes of heat transfer is the second source of uncertainties in these measurements. The transient heating of the wire

generates convection due to the turbulence that appears as a consequence of the different densities of the fluid thermal layer. The adjacent layers of the heated wire, at much higher temperature, experience a decrease in the density when compared with that of the bulk and, as a result, they move. This convective flux contributes to the energy transport, and the equations translating the conductive process are no longer valid.

The transient hot-wire method has the advantage of using short times to perform the measurement compared with times necessary for the onset of convection. Moreover, if this convection manifests itself, it can be detected. Once the onset of convection produces an increased transference of the heat from the wire, this results in an increase in the value of the thermal conductivity that can be detected by an analysis of the scattering plot of the deviations of the experimental ΔT as a function of the logarithm of time, visible as a concave curvature toward the time axis.

The heat transport by radiation that is associated with any measurement of thermal conductivity is easily treated if the fluid does not contribute directly or indirectly to the radiation process. In those cases, the fluid is transparent and limited by grey boundaries, the radiative heat transport is not associated with the conductive process, and the heat fluxes are additive. The evaluation of the corrections is easily treated. However, its size must be determined in high precision measurements. If we consider the radiative process between the tungsten wire and the cell wall as between diffusive grey surfaces, and because the area of heat transfer contained in the cell wall is much larger than the outer surface of the hot wire, the heat transfer is not a function of the emissivity of the cavity. Following the analysis presented by Siegel and Howell [24] and also described in [25], the resulting correction is

$$\delta T_5 = \frac{8\pi r_i \varepsilon_{\text{Tungsten}} \sigma T_0^3 \Delta T_{\text{id}}^2}{q}, \tag{3}$$

where σ is the Stefan–Boltzmann constant and $\varepsilon_{\text{Tungsten}}$ is the emissivity of tungsten, tabulated in [26]. The emissivity can be taken for polished tungsten, with an average value of 0.28, temperature independent. Keeping all the variables the same, the radiation correction is about four times greater at 200°C than at room temperature. This correction is of the order of 30 mK, for a temperature rise of 4 K. This is the formula that has to be applied for argon and dry air, considered as transparent fluids.

However, when the fluid absorbs or emits radiation, the conductive and radiative fluxes are associated and the analysis is difficult and presents itself as a numerical solution requiring the optical properties of the fluid and its boundaries. This might be the case for the humid air

measurements, to be presented later, namely for higher water concentrations, as water is known to absorb strongly in the infrared, emitting also in the same region.

A detailed analysis of the problem of radiation in the transient hot-wire method for absorbing fluids was performed by Menashe et al. [27], and Nieto de Castro et al. [28, 29] proposed an approximate analytical solution, stating that the effect of the radiative heat transport in the thermal conductivity measurements using the transient hot-wire technique is less affected by radiation than the stationary techniques. These last authors, based on the results of their analysis, suggest that if ΔT_{w} was to be fitted to an equation like

$$\Delta T_{\mathrm{w}} = C_1 \ln t + C_2 t + C_3. \tag{4}$$

Some considerations could be made concerning the influence of each term on the slope of the curve, concluding that, if the effect of the radiation was to be significant, it could be observed directly on the ΔT_{id} vs. ln t curve. As an example, measurements with liquid toluene at 550 K showed that a curvature of the order of 0.2% in the temperature rise gives a contribution of about 3% to the thermal conductivity [29].

The second source of uncertainty is caused by random and systematic errors. As mentioned before, in the transient hot-wire method the thermal conductivity is evaluated essentially by the determination of the temperature rise of a heat source as a function of time, following initiation of a current in it. This is achieved, in general, with two thin wires of different lengths – to eliminate the end effects – connected to different arms of an automatic dc Wheatstone bridge, as described elsewhere [30, 31]. For the predetermined duration of the experiment (normally 1 s), the imbalance of the bridge electric potential is measured every 2 ms. The application of Ohm's law to the bridge circuit gives the resistance increase of the heated wire, while a knowledge of the relation between the electrical resistance of the wire and its temperature allows us to obtain a set of points $(DeltaT_{\mathrm{id}}, \ln t_i)$ as required by the mathematical model. The final value of the experimental thermal conductivity is assessed by a function that incorporates uncorrelated input quantities that carry an associated uncertainty and that, in the end, will contribute to the global uncertainty of the measurement. As it is, the thermal conductivity can be represented by the equation,

$$\lambda = \lambda(t, \ell_{\mathrm{S}}, \ell_{\mathrm{L}}, R_{\mathrm{S}}, V, R_{\mathrm{L}}, R_2, \alpha, R_1, r_{\mathrm{i}}, T_0, C_p, \rho), \tag{5}$$

where t is the time, ℓ_{S} and ℓ_{L} are the lengths of the short and long wires, r_i is the wire radius, R_{S}, R_{L} are the short and long wire resistances, R_1, R_2

are the decade box resistances, V is the power supplied to the bridge, α is the temperature coefficient for the wire resistance, T_0 is the initial temperature of the fluid or "bath temperature," C_p is the heat capacity of the fluid, and ρ is its density.

Ramires and Nieto de Castro [22] have demonstrated that for measurements in liquid water performed with similar equipment, an uncertainty equal to $5.3 \times 10^{-3} \mathrm{W \cdot m^{-1} \cdot K^{-1}}$ was obtained. Using a coverage factor $k = 2$, the final value of the thermal conductivity estimate is $0.615 \mathrm{W \cdot m^{-1} \cdot K^{-1}}$, now represented as $0.615 \pm 0.011 \mathrm{W \cdot m^{-1} \cdot K^{-1}}$. However, it was also concluded from the values of the individual contributions of the input quantities to the final uncertainty of the output estimate, that the pseudo linear temperature resistance coefficient has a major effect on the final uncertainty of the thermal conductivity. No other uncertainty contributes so significantly to the final value, so the calibration of the wires must be performed very accurately. In the present instrument this calibration has to be made *in situ*, that is, with the wires already placed in the cells. However, this calibration depends also of the uncertainty of the decades used to balance the bridge, as the values of the equilibrium resistances are to be used in the calibration. High precision decades must therefore be used if we want to obtain highly accurate results in this operation. In addition, good stabilization of the temperature of the thermostatic bath is necessary, not only to avoid non-uniformities in temperature, which can cause the onset of convection, but also to know this value with great confidence.

Finally, a different step has to be made. During an experiment, the thermal conductivity and the heat capacity per unit volume ρC_P of the fluid vary with temperature. As explained in [21], if a linear perturbation of these properties about the equilibrium temperature T_0 is assumed, then both a time-dependent correction and a time-independent correction arise. The time-dependent contribution is most easily accounted for by referring the thermal conductivity determined from the slope of the line, ΔT_{id} vs. ln t, to a reference state $(T_{\mathrm{ref}}, \rho_{\mathrm{ref}})$, so that the basic Eq. (1) is maintained;

$$\Delta T_{\mathrm{id}} = \frac{q}{4\pi\lambda\,(T_{\mathrm{ref}}, \rho_{\mathrm{ref}})} \ln \frac{4kt}{r_{\mathrm{i}}^2 C}. \tag{6}$$

The reference temperature and density are given by

$$T_{\mathrm{ref}} = T_0 + \frac{1}{2}\left[\Delta T\,(t_{\mathrm{i}}) + \Delta T\,(t_{\mathrm{f}})\right], \tag{7}$$

$$\rho_{\mathrm{ref}} = \rho\,(T_{\mathrm{ref}}, P_0), \tag{8}$$

where t_i and t_f are the initial and final times of the measurement interval used in the regression line and P_0 is the equilibrium pressure of the fluid. The time-independent part is only important for thermal diffusivity measurements, as explained in [32].

3. INSTRUMENT

3.1. Cell Design and Construction

The cells were constructed of 316 stainless steel, have a cylindrical shape, split to open along the axial plane. One half cylinder has four wire ports, where stainless steel wire hooks of diameter 0.5 mm are located. This half cylinder has also several positions to adjust the height of the wire supports. When the two complementary halves are put together, two cylinder cavities of 10 mm in diameter and 210 mm in height are generated for the short and long tungsten wire. Figure 1 shows the measuring cells.

One of the most difficult operations is the tungsten wire solder connection to the wire supports in the cells. First, the tungsten wire is soldered to the cell top hook (B in Fig. 1). Second, an annealed tungsten tape, necessary to make the electrical contact without exerting any transversal force in the wire during heating, is soldered to a small weight, used to keep the wire vertical while heating. This ensemble is then soldered to the other end of the wire. Finally the tape is soldered to the bottom port of the cell. The same procedure is repeated with the short wire cell. The cells are then suspended and the wires lengths measured with a cathetometer to within 0.01 mm. The continuity of the circuit is checked, and the cells are then mounted to the top closure of the pressure vessel. The wires that exit the cell are then soldered to the cables that will cross the vessel cap to the outside bridge leads, sealed using a high pressure single wire seal (Conax Buffalo Technologies). All these leads are shielded and grounded to diminish the electrical noise. When the procedure was successful, the resistances of the wires and cables were checked, and the pressure vessel was closed and mounted in the furnace. Table I shows the characteristics of the thermal conductivity cells. The tungsten wire radius was measured using a scanning electron microscope.

3.2. Vessel and Furnace Design and Construction

The pressure vessel was also constructed of stainless steel 316. The high temperature furnace was constructed of a refractory ceramics, *Ceraboard 100* from Manville, with 7 cm thickness. This construction guarantees the temperature stability inside the vessel to be better than 0.01 K,

Fig. 1. Stainless steel measuring cells. A – cell top and also part of the sealing vessel cap. B – Soldering end supports for the wires: a stainless steel hook, tungsten tape, and small tungsten weight comprise the fixation mechanism.

Table I. Characteristics of the Thermal Conductivity Cells

Cell diameter	10.00 ± 0.01 mm
Tungsten-wire diameter	$8.94 \pm 0.05 \mu$m
Long-wire length at 293 K	71.69 ± 0.02 mm
Short-wire length at 293 K	148.92 ± 0.02 mm

Fig. 2. Pressure vessel and high temperature furnace.

between room temperature and 500 K. Figure 2 shows a view of the furnace open with the pressure vessel inside.

3.3. Automatic Wheatstone Bridge

The temperature rise of the wire as a function of time is determined by an automatic Wheatstone bridge, especially designed for this instrument. It is based on a previously constructed bridge for the high-temperature instrument for molten materials and was described in [33]. Some changes were introduced and will be described here. The most important are the power supply (Thurlby Thandar Instruments TSP3222) capable of being programmed and with dual operation symmetric to ground, the new MOSFET switch and its connection, and the number of

data points in a run. The power supply is controlled by an IEEE-488.2 interface, making it possible to obtain a resolution of 12 bits or 10 mV and an uncertainty of $\pm 0.05\%$. The values of the voltage measurements have a resolution of 5×10^{-6}V, given the resolution of the PC30AT data acquisition board and the amplification gain. The resolution in the resistance measurement in the bridge circuit is of the order of 4 mΩ. The general layout of the measuring circuit is shown in Fig. 3, linked to the computer CPU for control and measurement. The digital multimeter is a HP 34401A. As shown, the MOSFET switch applies power symmetrically about ground, to reduce parasitic potentials and noise.

The bridge layout is shown is Fig. 4. The resistance distribution in the bridge circuit must obey certain criteria to compensate for the contact potential effects in the wires and contact resistances and to generate constant heat flux dissipation during a measurement. Two decade resistance boxes (CROPICO RBB6B), with six decades and a minimum step of 0.001Ω, are identified by R_1 and R_2, the short and long wires by R_S and R_L and the corresponding lead resistances by R_{S1}, R_{S2}, R_{L1}, and R_{L2}. In one of the arms, a standard resistor of 10Ω (R_{std}) is used to measure the current in the bridge. In the inactive arm of the bridge, two nearly equal resistances (R_3 and R_4) of 330Ω each provide the reference point for the bridge near ground. The points L/H represent voltage-measuring points for the digital multimeter that are controlled by the multiplexer.

The bridge is initially balanced, having a long tungsten wire in one arm, and a short compensating tungsten wire in the adjacent arm. The PC30AT board measures the imbalance and these imbalance voltages due to the changes in the resistance of the tungsten wires are transformed to

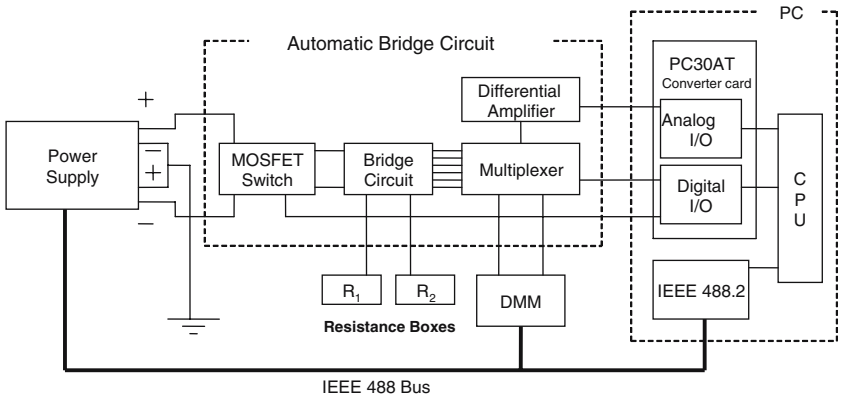

Fig. 3. Measuring circuit.

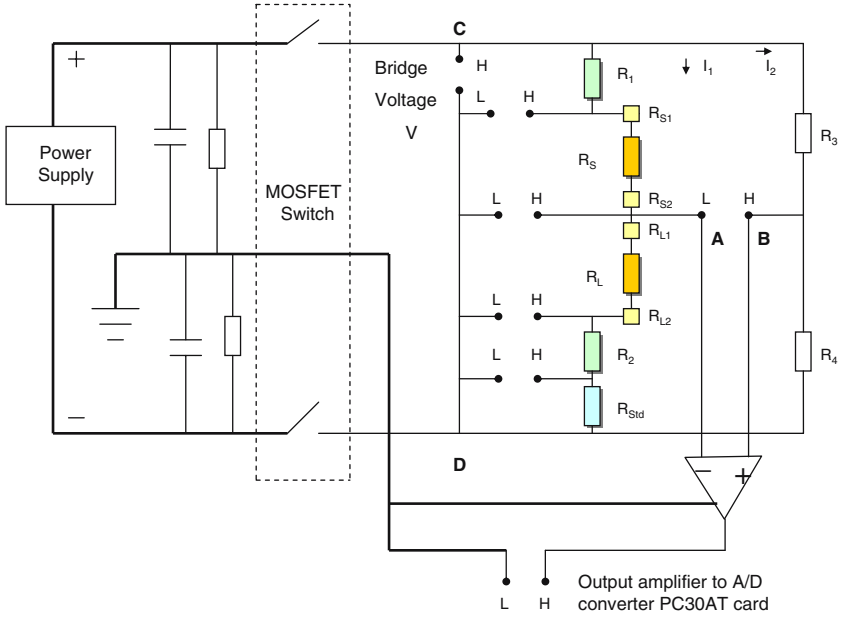

Fig. 4. Simplified schematic of the bridge circuit.

resistance increases by the bridge equation of the circuit. The MOSFET switch also has a residual resistance of 0.6Ω, which must be taken into account. After the resistance of the tungsten wire is calibrated as a function of temperature, a process described below, we can obtain the temperature rise in the wire as a function of time, proceed with application of the corrections, and fit the regression line to obtain the thermal conductivity from the slope. The bridge can also operate in a steady-state mode, permitting the measurement of all the resistances with a very low current for the *in situ* calibration of the wires and to check for the end effect compensation. The ratios $\sigma_i = \frac{R_i}{\ell_i}$, where R is the resistance and ℓ the length, with the subscript i designating the long or short wire, never deviate for our wires by more than 0.03% [21].[2]

3.4. Ancillary Equipment

In order to fill and pressurize the cell, a standard gas/liquid filling system has been assembled, as shown in Fig. 5. The system is capable of filling a gas or a liquid, pressurizing the gas or the liquid, over the

[2] As explained in [21], a deviation up to 0.2% is tolerable.

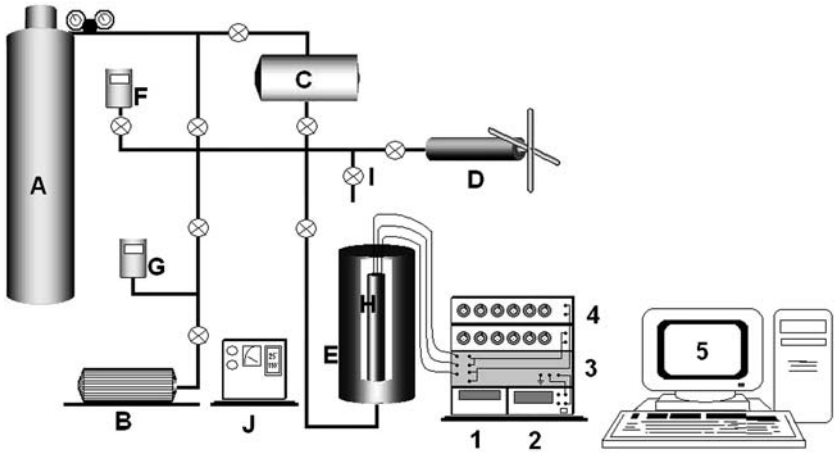

Fig. 5. Gas/liquid filling system (schematic). A – gas cylinder, B – vacuum pump, C – gas compressor, D – manual pump for compressing liquid or gas compressor, E – furnace, F – pressure sensor, G – vacuum sensor, H – pressure cylinder, I – vent, J – furnace power and controller unit. Numbers refer to the measuring system. 1 – power supply, 2 – digital multimeter, 3 – thermal conductivity bridge, 4 – resistance boxes, 5 – personal computer.

pressure range 0–70 MPa. A high-pressure system composed of a HIP manual liquid-pressure generator (HIP 62-6-10) rated for 70 MPa and an air-operated, diaphragm-type compressor (Newport Scientific 46-14-021-2) rated for 150 MPa is used. The pressure was measured with a pressure transducer (Setra Systems Datum 2000, with a sensor C206), calibrated in the Centro Español de Metrología, Madrid, with an uncertainty of 0.03 MPa at low pressures and 0.01 MPa at 70 MPa. The temperature of the cell is measured with a Pt100, calibrated in the laboratory, by transfer of a Class A secondary standard Pt100, from 0 to 158°C, to 0.05 K uncertainty. The system is also equipped with vacuum pumps.

A photograph of the complete layout of the equipment is shown in Fig. 6.

3.5. Calibration of the Tungsten Hot-Wire Resistive Properties as a Function of Temperature

As described in the "Introduction", the wires need to be calibrated as a function of temperature, to obtain the coefficient of variation of the resistance with temperature, per unit temperature, α. A preliminary calibration was made, for the range 25–113°C. Because the wires have been broken and had to be replaced with a different wire sample, an *in situ* calibration was made for the range 27–200°C, by using the bridge data in

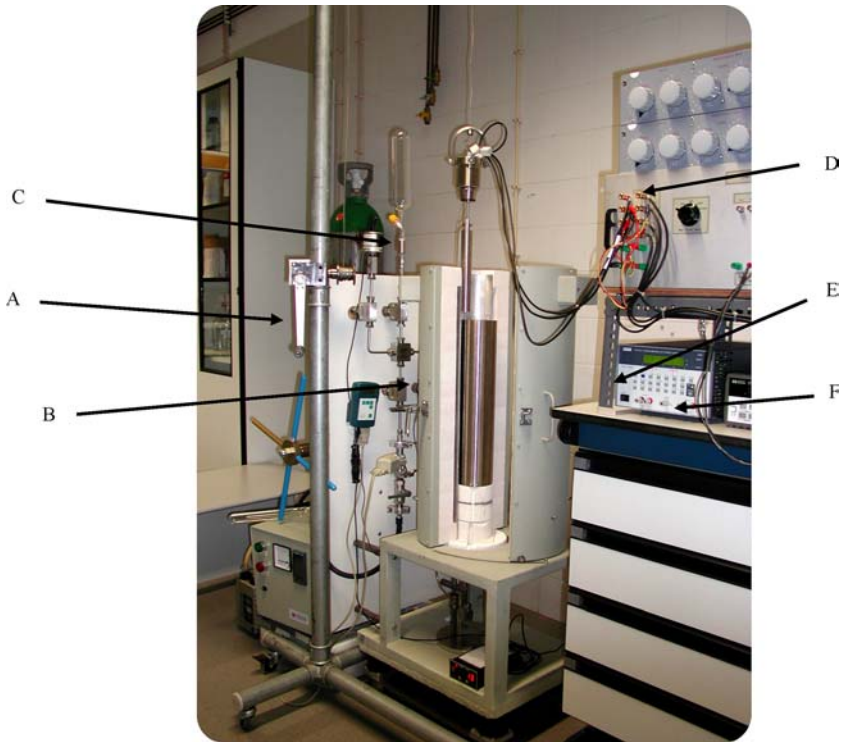

Fig. 6. General view of the equipment, including the filling and pressurizing zone. (A) high temperature furnace; (B) high pressure vessel; (C) measuring cell and electronic instrumentation, namely, the measuring bridge (D); (E) power supply and (F) multimeter. The Data acquisition system is mounted on a desktop, which sets beside the bridge.

the "steady-state" mode. The coefficient α showed a variability of about 3% between different wire samples, which requires a calibration each time a wire is replaced.[3] Figure 7 shows a typical calibration plot deviation, completely described in [33]. The deviations from an equation of the type,

$$\frac{R}{R_0} = 1 + \alpha\,(T - T_0) + \beta\,(T - T_0)^2 \tag{9}$$

with $\alpha = 3.3733 \times 10^{-3} \pm 9.7 \times 10^{-7}$ and $\beta = 1.723 \times 10^{-6} \pm 8.7 \times 10^{-8}$, are not greater than 0.04%.

[3] In fact, this operation must also be done to check for the agreement of the resistances per unit length of both wires.

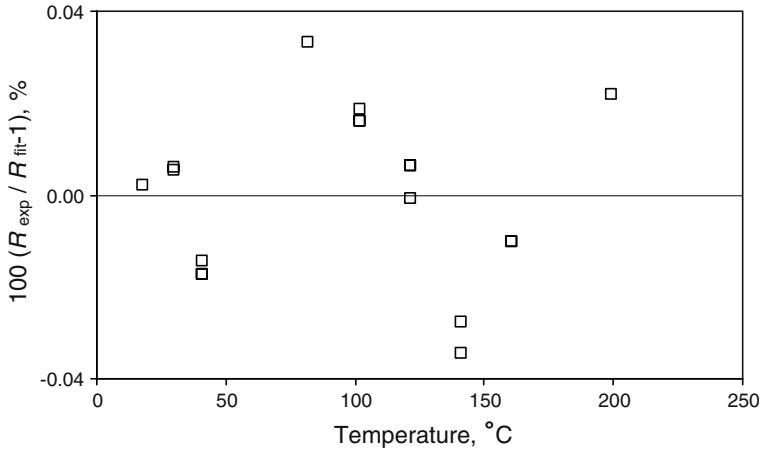

Fig. 7. Deviation between the experimental points and Eq. (9) for the calibration of the tungsten wire.

4. RESULTS

In order to test the accuracy of the measurements with the new equipment, measurements with gaseous argon, a reference gas for thermal conductivity measurements, have been performed, at six different temperatures and several pressure levels. An optimal choice of the temperature rise was made, using different power levels (typically generating temperature rises from 4 to 8 K), to test the performance of the equipment. A typical plot of the temperature increase in the hot wire, as a function of $\ln t$ is shown in Fig. 8, for a run at 300.28 K and 1.56 MPa. Figure 9 shows the plot over the analysis range, and the scattering diagram, representing, in percentage, the deviations between the measured temperature rises after all corrections, and the ideal model ΔT_{id}, for this run. It can be seen that after the corrections to the experimental measured temperature rise, the plot is linear, after 100 ms. The average deviation is 0.2%, with few points showing a scatter greater than 0.5%. This indicates yet some noise in the bridge that can be decreased by a better shielding of the cables, which will be done in the near future. As shown in Figs. 8 and 9, the measurement obeys the mathematical description of it, and can therefore be validated.

Measurements with argon were performed for several temperatures between room temperature and 200°C, for different pressure levels. Table II lists the experimental data for the six isotherms studied, at 304.80, 329.00, 360.05, 389.30, 417.50, and 475.70 K. The tables include the thermal conductivity at the reference state, $\lambda(T_{ref}, \rho_{ref})$ as well as the thermal

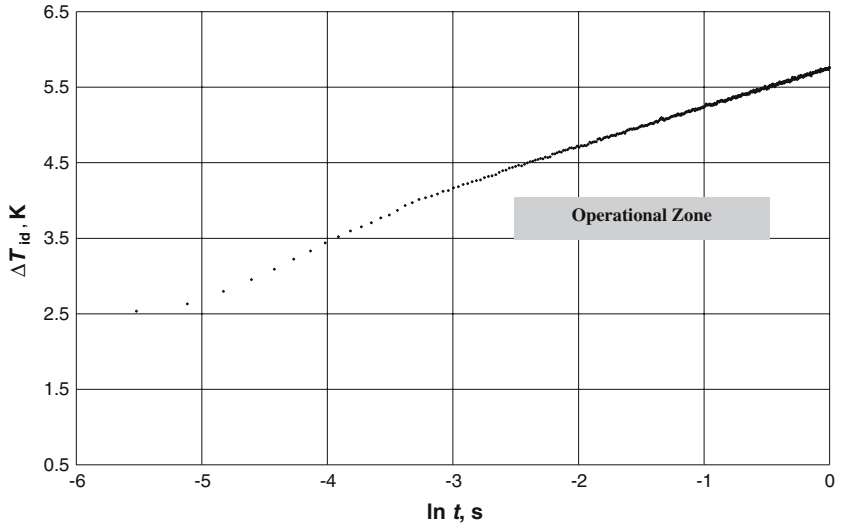

Fig. 8. Typical transient hot-wire experiment for gaseous argon, at 300.28 K and 1.56 MPa. The line is linear after 100 ms, the operational zone, from where the regression analysis shows that Eq. (4) is obeyed, with $C_2 = C_3 = 0$.

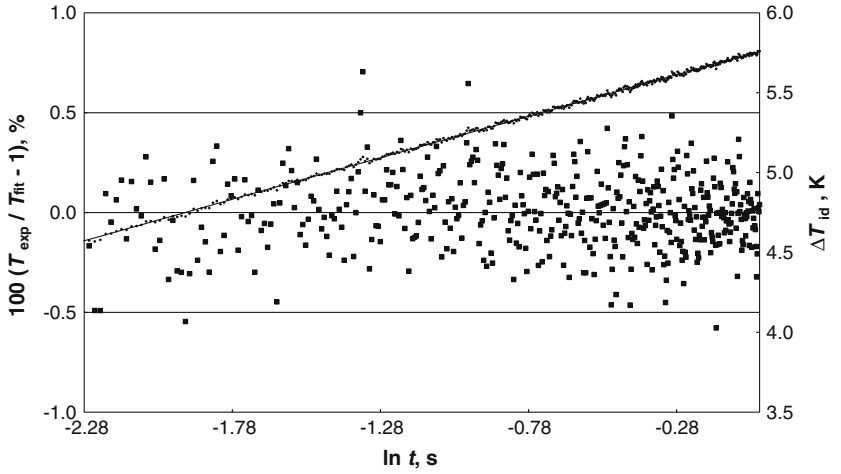

Fig. 9. Typical transient hot-wire experiment for gaseous argon, at 300.28 K and 1.56 MPa, showing the scattering diagram – deviations, in percentage, between ΔT_{id} and the regression line points. Right scale shows the real line, $\Delta T_{id} = f(\ln t)$.

conductivity corrected to a nominal temperature T_{nom}. The correction was applied in the form,

$$\lambda\,(T_{\text{nom}}, \rho_{\text{ref}}) = \lambda\,(T_{\text{ref}}, \rho_{\text{ref}}) + \left(\frac{\partial \lambda}{\partial T}\right)_{\rho_{\text{ref}}} (T_{\text{nom}} - T_{\text{ref}})\,. \tag{10}$$

Table II. Thermal Conductivity of Argon

P (MPa)	ρ_{ref} (kg·m^{-3})	T_{ref} (K)	$\lambda(T_{\text{ref}}, \rho_{\text{ref}})$ (mW·m^{-1}·K^{-1})	$\lambda\ (T_{\text{nom}}, \rho_{\text{ref}})$ (mW·m^{-1}·K^{-1})
		$T_{\text{nom}} = 304.80$ K		
1.02	16.12	305.82	18.16	18.21
1.56	24.71	305.54	18.30	18.35
2.32	37.02	305.26	18.64	18.69
2.59	41.36	305.27	18.72	18.77
4.47	72.14	304.80	19.59	19.59
		$T_{\text{nom}} = 329.00$ K		
1.20	17.55	329.88	19.25	19.30
1.27	18.58	329.53	19.48	19.53
1.96	28.73	329.63	19.74	19.78
2.34	34.39	329.16	19.90	19.95
3.03	44.64	329.00	20.16	20.16
3.63	53.54	329.21	20.25	20.30
5.98	88.98	328.48	21.13	21.18
7.32	109.35	328.27	21.87	21.92
		$T_{\text{nom}} = 360.05$ K		
1.24	16.58	360.36	20.82	20.86
1.56	20.84	360.22	20.94	20.98
1.64	21.95	360.22	20.99	21.04
2.24	30.01	360.05	21.29	21.29
3.20	42.92	359.83	21.53	21.58
4.16	55.88	359.59	21.87	21.92
8.72	117.56	359.06	23.85	23.90
		$T_{\text{nom}} = 389.30$ K		
1.39	17.18	389.74	22.22	22.27
2.14	26.39	389.51	22.50	22.55
2.78	34.32	389.39	22.72	22.76
3.33	41.14	389.30	22.88	22.88
3.56	43.96	389.24	22.99	23.04
4.19	51.72	389.17	23.18	23.23
5.35	66.13	389.04	23.48	23.53
6.05	74.81	388.99	23.80	23.85
6.66	82.29	388.94	24.01	24.05
7.50	92.66	388.86	24.26	24.30
8.26	101.98	388.79	24.61	24.66
8.50	104.95	388.78	24.58	24.63

Table II. (*Continued*)

P (MPa)	ρ_{ref} (kg·m^{-3})	T_{ref} (K)	$\lambda(T_{ref}, \rho_{ref})$ (mW·m^{-1}·K^{-1})	$\lambda\ (T_{nom}, \rho_{ref})$ (mW·m^{-1}·K^{-1})
		$T_{nom} = 417.50$ K		
1.21	13.85	418.35	23.32	23.36
1.40	16.07	418.38	23.39	23.43
2.11	24.22	418.21	23.65	23.69
2.74	31.49	418.12	23.90	23.95
3.42	39.24	418.02	24.11	24.15
4.13	47.37	417.94	24.28	24.32
4.80	55.03	417.79	24.54	24.59
5.47	62.76	417.62	24.74	24.78
6.18	70.78	417.57	24.99	25.04
6.89	78.86	417.50	25.21	25.21
7.58	86.69	417.44	25.57	25.60
8.27	94.50	417.39	25.72	25.77
		$T_{nom} = 475.70$ K		
1.09	10.97	476.58	25.58	25.62
1.41	14.22	476.54	25.71	25.75
2.12	21.28	476.42	26.04	26.08
2.79	28.04	476.38	26.31	26.36
3.52	35.28	476.21	26.47	26.52
4.25	42.57	476.08	26.79	26.83
5.01	50.18	476.04	26.87	26.92
6.10	60.90	476.43	27.37	27.42
7.98	79.51	475.70	27.89	27.89

The values of the temperature dependence of the thermal conductivity were estimated from the NIST REFPROP equation of state [34]. None of these corrections amount to more than ±1%, so that the contribution of uncertainties to the reported thermal conductivities is smaller than 0.1%.

For a moderately dense gas the thermal conductivity can be expanded in terms of density to the first order, i.e.,

$$\lambda(T, \rho) = \lambda_0(T) + \lambda_1(T)\,\rho + \ldots \tag{11}$$

The data for argon were represented as a linear function of density for all the temperatures. Table III shows the regression coefficients obtained and the corresponding errors,[4] commensurate with the estimated uncertainty of the experimental data. Table III also presents the result of the linear

[4] The errors are expressed as the root-mean-square deviations of the fit and of the coefficients.

Table III. Data Analysis of the Thermal Conductivity of Argon

T_{nom} (K)	σ (mW·m^{-1}·K^{-1})	λ_0 (mW·m^{-1}·K^{-1})	σ_{λ_0} (mW·m^{-1}·K^{-1})	λ_1 (mW·m^{-1}·K^{-1}·MPa^{-1})	σ_{λ_1} (mW·m^{-1}·K^{-1}·MPa^{-1})
Linear regression of the thermal conductivity (mW·m^{-1}·K^{-1}) against pressure (MPa)					
304.80	0.041	17.752	0.041	0.4053	0.015
329.00	0.100	18.960	0.067	0.3912	0.017
360.05	0.060	20.344	0.038	0.4030	0.009
389.30	0.043	21.808	0.029	0.3361	0.005
417.50	0.045	22.971	0.029	0.3365	0.006
475.70	0.080	25.351	0.055	0.3273	0.013
T_{nom} (K)	σ (mW·m^{-1}·K^{-1})	λ_0 (mW·m^{-1}·K^{-1})	σ_{λ_0} (mW·m^{-1}·K^{-1})	λ_1 (mW·m^{2}·kg^{-1}·K^{-1})	σ_{λ_1} (mW·m^{2}·kg^{-1}·K^{-1})
Linear regression of the thermal conductivity (mW·m^{-1}·K^{-1}) against reference density (kg·m^{-3})					
304.80	0.038	17.766	0.038	0.0250	0.001
329.00	0.099	18.975	0.065	0.0261	0.001
360.05	0.059	20.351	0.037	0.0298	0.007
389.30	0.043	21.807	0.029	0.0272	0.000
417.50	0.046	22.967	0.029	0.0294	0.001
475.70	0.079	25.343	0.054	0.0329	0.001

regression of the thermal conductivity with pressure, herein presented for engineering applications.

The data could be compared with many different sources of the thermal conductivity of argon gas, including several measurements made in this laboratory. However, a recent data comparison by NIST [34] produced with a maximum 2% uncertainty, permits a faster comparison of our data. Figure 10 shows this comparison. The values of the thermal conductivity measurements for argon agree within 0.9% ($k=2$) with the best reference measurements endorsed by IUPAC [21], with an uncertainty of 0.6% ($k=2$), and with the NIST REFPROP equation (estimated 2% uncertainty) to within 1% [34].

These results, associated with the detailed uncertainty analysis previously described, support the claim or assertion that the uncertainty of the present data is of the order of 1% ($k=2$).

The measurements with dry air (no traces of water present) were performed on a synthetic mixture produced by Linde AG, Wiesbaden,

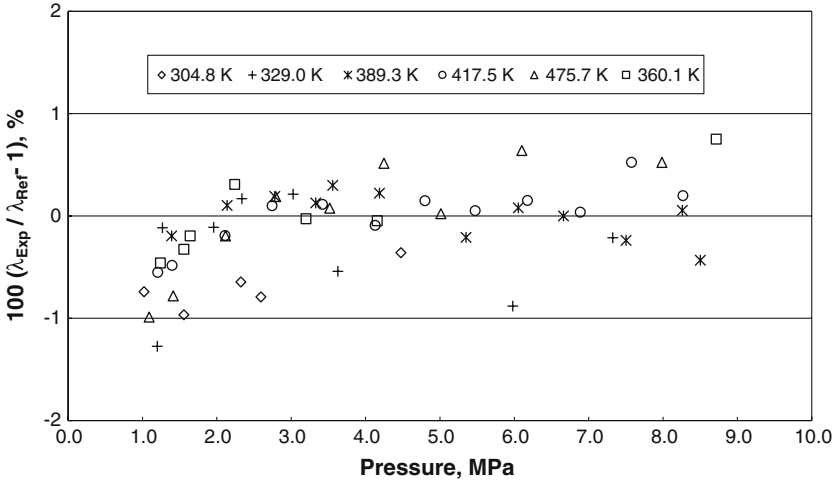

Fig. 10. Comparisons between the measured argon thermal conductivity data with values calculated with NIST REFPROP [34].

Germany. The certified molar composition of this mixture is: Argon – 0.00920; Oxygen – 0.20966; Nitrogen – 0.78114. The measurements were performed for three isotherms, 316.20, 377.60, and 436.00 K, and pressures up to 10 MPa. The results are presented in Table IV, including the thermal conductivity at the reference state, $\lambda(T_{\mathrm{ref}}, \rho_{\mathrm{ref}})$ as well as the thermal conductivity corrected to a nominal temperature $T_{\mathrm{nom},}$, computed by using Eq. (10). The values of the temperature dependence of the thermal conductivity were also estimated from the NIST REFPROP equation of state [34]. None of these corrections amount to more than $\pm 1\%$, so that the contribution of uncertainties to the reported thermal conductivities is smaller than 0.1%.

The data for dry air were represented as a linear function of density for all the temperatures. Table V shows the regression coefficients obtained and the corresponding errors,[4] commensurate with the estimated uncertainty of the experimental data. Table V also presents the result of the linear regression of the thermal conductivity on pressure, herein presented for engineering applications. Figure 11 shows the plot of the thermal conductivity of air as a function of density, for the three isotherms. This dependence is found to be linear, as expected for the low and moderate densities of the measurements, although a small curvature for the lowest temperature can be discerned. However, no statistical improvement was found with a quadratic fit.

Table IV. Thermal Conductivity of Dry Air

P (MPa)	ρ_{ref} (K)	T_{ref} (kg·m^{-3})	$\lambda(T_{ref}, \rho_{ref})$ (mW·m^{-1}·K^{-1})	$\lambda(T_{nom}, \rho_{ref})$ (mW·m^{-1}·K^{-1})
		$T_{nom} = 316.20$ K		
1.03	11.37	317.33	27.33	27.40
1.12	12.29	317.14	27.28	27.35
1.43	15.70	317.13	27.50	27.57
2.08	22.94	316.91	27.80	27.86
2.72	29.95	316.82	28.04	28.11
3.49	38.49	316.73	28.31	28.37
4.30	47.49	316.63	28.73	28.79
4.93	54.42	316.55	29.07	29.13
5.62	62.03	316.48	29.33	29.39
6.54	72.20	316.40	29.84	29.89
7.34	80.90	316.36	30.33	30.38
7.89	86.91	316.40	30.54	30.60
8.67	95.38	316.38	31.09	31.14
9.33	102.58	316.28	31.59	31.63
10.22	112.17	316.20	32.00	32.00
		$T_{nom} = 377.60$ K		
1.20	11.03	378.13	31.17	31.23
1.88	17.23	377.89	31.63	31.69
1.90	17.42	377.91	31.74	31.80
2.73	25.05	377.86	31.79	31.85
3.45	31.58	377.81	32.24	32.31
4.15	37.98	377.73	32.52	32.58
4.82	44.03	377.67	32.76	32.83
5.52	50.37	377.61	32.94	33.04
6.21	56.56	377.60	33.27	33.27
		$T_{nom} = 377.60$ K		
6.93	62.97	377.56	33.57	33.62
7.67	69.59	377.51	33.80	33.85
8.42	76.17	377.45	33.97	34.02
8.94	80.77	377.46	34.37	34.43
9.31	84.03	377.46	34.70	34.76
10.13	91.13	377.39	34.92	34.97
		$T_{nom} = 436.00$ K		
1.25	9.99	436.09	34.82	34.89
1.99	15.77	436.00	35.25	35.25
3.24	25.64	435.90	35.65	35.71
4.08	32.22	435.82	35.94	36.00
5.02	39.50	435.78	36.28	36.34
5.91	46.35	435.79	36.62	36.68
6.67	52.17	435.70	36.91	36.96
8.51	66.14	435.55	37.50	37.56
9.87	76.27	435.63	37.94	37.99

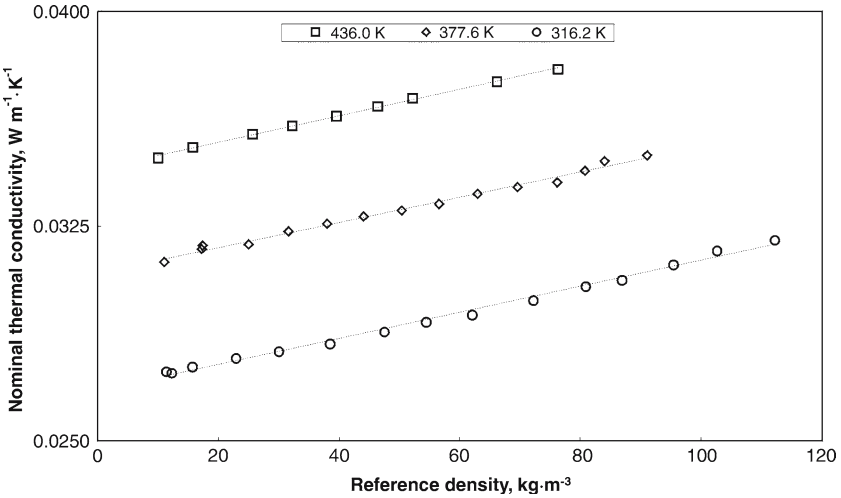

Fig. 11. Variation of the thermal conductivity of dry air with density, for the three nominal temperatures.

Table V. Data Analysis of the Thermal Conductivity of Dry Air

T_{nom} (K)	σ (mW·m^{-1}·K^{-1})	λ_0 (mW·m^{-1}·K^{-1})	σ_{λ_0} (mW·m^{-1}·K^{-1})	λ_1 (mW·m^{-1}·K^{-1}·MPa^{-1})	σ_{λ_1} (mW·m^{-1}·K^{-1}·MPa^{-1})
Linear regression of the thermal conductivity (mW·m^{-1}·K^{-1}) against pressure (MPa)					
316.20	0.122	26.743	0.062	0.5012	0.011
377.60	0.112	30.881	0.063	0.3967	0.010
436.00	0.051	34.528	0.036	0.3576	0.006
T_{nom} (K)	σ (mW·m^{-1}·K^{-1})	λ_0 (mW·m^{-1}·K^{-1})	σ_{λ_0} (mW·m^{-1}·K^{-1})	λ_1 (mW·m^{2}·kg^{-1}·K^{-1})	σ_{λ_1} (mW·m^{2}·kg^{-1}·K^{-1})
Linear regression of the thermal conductivity (mW·m^{-1}·K^{-1}) against reference density (kg·m^{-3})					
316.20	0.127	26.739	0.065	0.0456	0.001
377.60	0.114	30.858	0.065	0.0442	0.001
436.00	0.042	34.498	0.030	0.0464	0.001

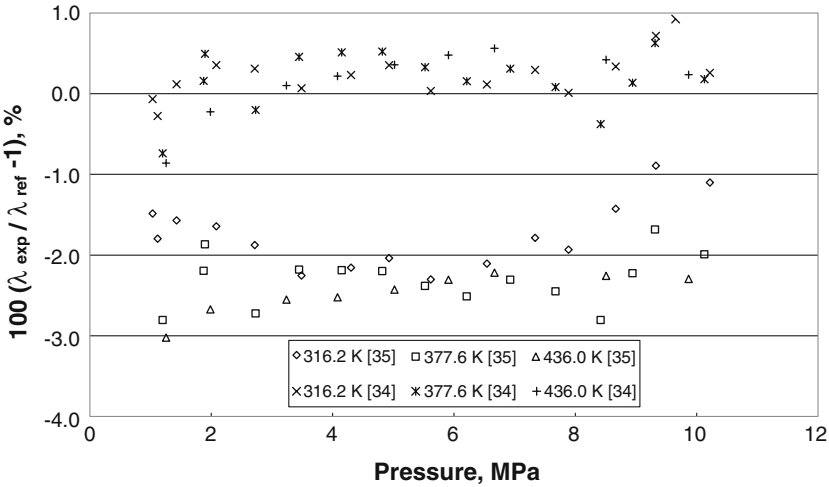

Fig. 12. Comparisons between the measured dry air thermal conductivity data, NIST REFPROP [34], and Stephan and Laesecke correlation [35].

Figure 12 shows comparisons among the measured data, NIST REFPROP [34], and a correlation previously presented by Stephan and Laesecke [35]. As found for argon, the results of the NIST property package do not deviate from our data by more than 1%. The correlation of Stephan and Laesecke deviates from our data between -1% and -3%, a figure that is commensurate with the uncertainty of their correlation in this temperature and pressure range. These results, associated with the detailed uncertainty analysis previously described for argon, support the claim that the uncertainty of the present data for dry air is of the order of 1% ($k = 2$).

5. CONCLUSIONS

New equipment for the measurement of the thermal conductivity of gases and liquids has been constructed and commissioned. It has been validated with measurements on gaseous argon and found to have an estimated uncertainty of 1%, ISO definition (coverage factor $k = 2$). Measurements on dry air, for the temperatures 316.20, 377.60, and 436.00 K, and for pressures up to 10 MPa were also presented, with an estimated uncertainty of 1% ($k = 2$).

We hope in the near future to extend the temperature range of the instrument to lower temperatures and higher pressures and to make

measurements with humid air and other fluids. We also expect that molecular interpretations of the first density coefficient of the thermal conductivity [36], will be presented.

ACKNOWLEDGMENTS

Most of this work was performed before our beloved colleague and friend, Prof. Maria de Lurdes Ramires, passed away in the spring of 2004. She was supervising the Ph. D. work of Ms. S.G.S. Beirão, when she passed away. We would like to pay her a tribute for all the excellent scientific work she has done in the past and all the friendship she has given to us. One of us (S.G.S. Beirão) wants to thank Fundação para a Ciência e a Tecnologia for the Ph.D. grant PRAXIS XXI/BD/14765/96. This work was partially financed by project POCTI/FIS/19/2001, from Fundação para a Ciência e a Tecnologia, Portugal and European project NNE5-2001-00473, "Advanced Adiabatic Compressed Air Energy Storage".

REFERENCES

1. C. A. Nieto de Castro, J. C. G. Calado, W. A. Wakeham, and M. Dix, *J. Phys. E, Sci. Instr.* **9**:1073 (1976).
2. C. A. Nieto de Castro, J. C. G. Calado, and W. A. Wakeham, *Proc. 7th Symp. Therm. Prop.*, A. Cezairliyan, ed. (ASME, New York, 1977), pp. 247–253.
3. C. A. Nieto de Castro, J. M. N. A. Fareleira, J. C. G. Calado, and W. A. Wakeham, *Proc. 8th Symp. Prop.*, J. V. Sengers, ed. (ASME, New York, 1982), pp. 730–738.
4. J. C. G. Calado, J. M. N. A. Fareleira, C. A. Nieto de Castro, and W. A. Wakeham, *Int. J. Thermophys.* **4**:193 (1983).
5. J. C. G. Calado, U. V. Mardolcar, J. M. N. A. Fareleira, and C. A. Nieto de Castro, *Int. J. Thermophys.* **9**:351 (1988).
6. U. V. Mardolcar, J. M. N. A. Fareleira, C. A. Nieto de Castro, and W. A. Wakeham, *High Temp. High Press.* **17**:469 (1985).
7. U. V. Mardolcar, C. A. Nieto de Castro, and W. A. Wakeham, *Int. J. Thermophys.* **7**: 259 (1986).
8. J. C. G. Calado, U. V. Mardolcar, C. A. Nieto de Castro, H. M. Roder, and W. A. Wakeham, *Physica* **143A**:314 (1987).
9. U. V. Mardolcar and C. A. Nieto de Castro, *Ber. Bunsenges. Phys. Chem.* **91**:152 (1987).
10. N. Gurova, M. T. Barão, U. V. Mardolcar, and C. A. Nieto de Castro, *High Temp.-High Press.* **26**:25 (1994).
11. A. N. Gurova, C. A. Nieto de Castro, and U. V. Mardolcar, *Thermal Conductivity 22*, T. W. Tong, ed. (Technomic Pubs. Co., Lancaster, Pensylvania, 1994), pp. 189–199.
12. A. N. Gurova, C. A. Nieto de Castro, and U. V. Mardolcar, *Int. J. Thermophys.* **18**:1077 (1997).
13. A. N. Gurova, U. V. Mardolcar, and C. A. Nieto de Castro, *Int. J. Thermophys.* **20**:63 (1999).
14. M. L. V. Ramires, J. M. N. A. Fareleira, C. A. Nieto de Castro, M. Dix, and W. A. Wakeham, *Int. J. Thermophys.* **14**:1119 (1993).

15. M. L. V. Ramires, C. A. Nieto de Castro, J. M. N. A. Fareleira, and W. A. Wakeham, *J. Chem. Eng. Data* **39**:186 (1994).
16. M. L. V. Ramires and C. A. Nieto de Castro, *Int. J. Thermophys.***21**:671 (2000).
17. C. A. Nieto de Castro, S. F. Y. Li, A. Nagashima, R. D. Trengove, and W. A. Wakeham, *J. Phys. Chem. Ref. Data* **15**:1073 (1986).
18. M. L. V. Ramires, C. A. Nieto de Castro, R. A. Perkins, Y. Nagasaka, A. Nagashima, M. J. Assael, and W. A. Wakeham, *J. Phys. Chem. Ref. Data* **29**:133 (2000).
19. M. J. Assael, C. A. Nieto de Castro, M. L. V. Ramires, and W. A. Wakeham, *J. Phys. Chem. Ref. Data* **19**:113 (1990).
20. M. L. V. Ramires. C. A. Nieto de Castro, Y. Nagasaka, A. Nagashima, M. J. Assael, and W. A. Wakeham, *J. Phys. Chem. Ref. Data* **24**:1377 (1995).
21. M. J. Assael, C. A. Nieto de Castro, H. M. Roder, and W. A. Wakeham, *Experimental Chemical Thermodynamics*, Vol. 2, *Measurement of the Transport Properties of Fluids*, Chap. 7, W. A. Wakeham, A. Nagashima, and J. V. Sengers, eds. (Blackwells, Oxford, 1991).
22. M. L. V. Ramires and C. A. Nieto de Castro, *Proc. TEMPMEKO 2001*, *8*th *Int. Symp. Temp. Therm.Measurements in Ind. and Sci.*, B. Fellmuth, J. Seidel, and G. Scholz, eds. (VDE VERLAG GmbH, Berlin, Germany, 2002), Vol. 2, p. 1181.
23. C. A. Nieto de Castro, B. Taxis, H. M. Roder, and W. A. Wakeham, *Int. J. Thermophys.* **9**:293 (1988).
24. R. Siegel and J. R. Howell, *Thermal Radiation Heat Transfer*", 2nd Ed. (Hemisphere, New York, 1981).
25. R. A. Perkins, H. M. Roder, and C. A. Nieto de Castro, *J. Res. Natl. Inst. Stand. Technol.* **96**:247 (1991).
26. Y. S. Touloukian and D. P. DeWitt, *Thermal Radiative Properties – Metallic Elements and Alloys* (Plenum, New York, 1970).
27. J. Menashe and W. A. Wakeham, *Int. J. Heat Mass Transfer* **25:**461 (1982).
28. C. A. Nieto de Castro, S. F. Y. Li, G. C. Maitland, and W. A. Wakeham, *Int. J. Thermophys.* **4:**311 (1983).
29. C. A. Nieto de Castro, R. A. Perkins, and H. M. Roder, *Int. J. Thermophys.* **12**:985 (1991).
30. M. L. V. Ramires, *Medida Experimental de Condutibilidade Térmica de Liquidos Condutores pelo Método do Fio Aquecido em Regime Transiente*, Ph.D. Thesis (University of Lisbon, 1992).
31. M. L. V. Ramires, J. M. N. A. Fareleira, C. A. Nieto de Castro, M. Dix, and W. A. Wakeham, *Int. J. Thermophys.* **14**:1119 (1993).
32. M. J. Assael, M. Dix, I. Drummond, L. Karagiannidis, M. J. Lourenço, C. A. Nieto de Castro, M. Papadaki, M. L. Ramires, H. van den Berg, and W. A. Wakeham, *Int. J. Thermophys.*, **18**:439 (1997).
33. S. G. S. Beirão, *Condutibilidade Térmica de Fluidos em Gamas Alargadas de Temperatura e Pressão*, Ph.D. Thesis (University of Lisbon, 2006)
34. E. W. Lemmon, M. O. McLinden, and M. L. Huber, *REFPROP Version 7* (National Inst. Stand. Tech., Gaithersburg, Maryland, 2002).
35. K. Stephan and A. Laesecke, *J. Phys. Chem. Ref. Data* **14**:227 (1985).
36. C. A. Nieto de Castro, D. G. Friend, R. A. Perkins, and J. C. Rainwater, *Chem. Phys.* **145**:19 (1990).